Electronic Supplementary Material (ESI) for Nanoscale.

Supplementary Information

Stress-Engineered Palladium Nanowire for Wide Range (0.1%–3.9%) of H_2 Detection with High Durability

Jae-Shin Lee†‡, Min-Ho Seo†‖‡, Kwang-Wook Choi†, Jae-Young Yoo†, Min-Seung Jo† and Jun-Bo Yoon†*

†School of Electrical Engineering, Korea Advanced Institute of Science and Technology (KAIST), 291 Daehak-ro, Yuseong-gu, Daejeon 34141, Republic of Korea

‖Information & Electronics Research Institute Korea Advanced Institute of Science and Technology (KAIST), 291, Daehak-ro, Yuseong-gu, Daejeon 34141, Republic of Korea

‡These authors contributed equally to this work.

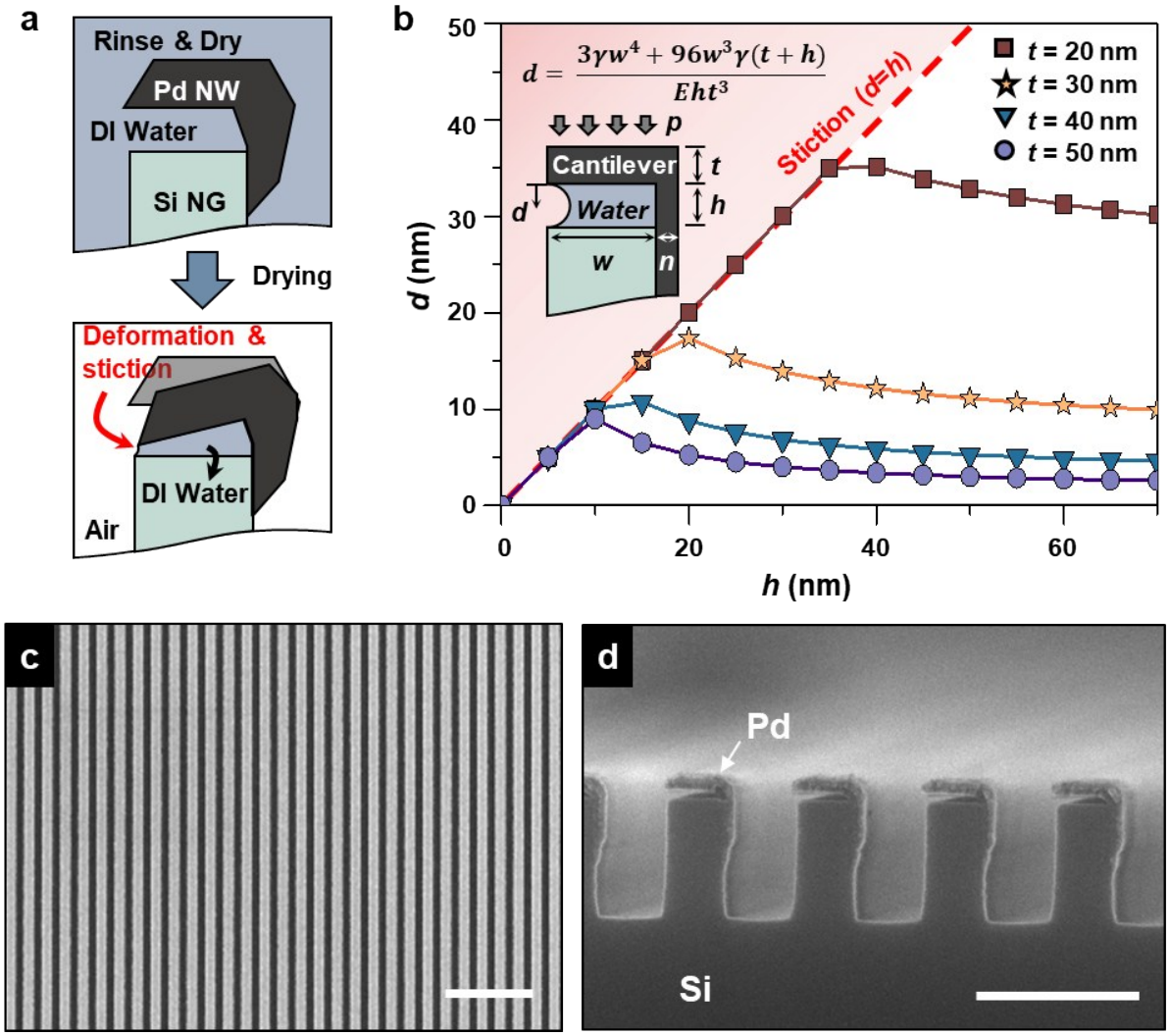

Figure S1. (a) Schematic description of the fabrication failure caused by stiction of PA-PdNW. When the bending of the air-suspended part of the PA-PdNW due to the capillary force developed in the water drying process exceeds the air-gap height, a contact between the substrate and the PA-PdNW happens and stiction can occur. (b) Graph showing the calculated bending of PA-PdNW with various thickness and air-gap height. The inset figure and equation describe the simplified model and corresponding bending. Shaded region represents PA-PdNW design specifications at risk of stiction failure. (c-d) SEM images of fabricated PA-PdNW with wire thickness of ~30 nm and air-gap of ~20 nm. (c) A top-view (Scale bar = 2 μm) and (d) a cross-section view (Scale bar = 500 nm) of the fabricated PA-PdNW array.

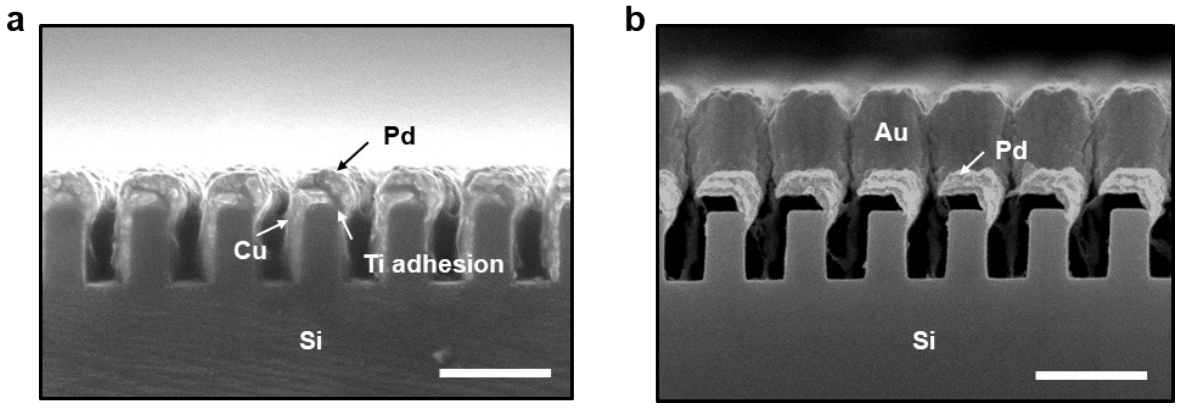

Figure S2. Cross-sectional SEM image taken after (a) the 3rd step and (b) the 6th step (Scale bars = 500 nm). (a) The boundary between Pd and Cu layers can be found clearly along the Ti adhesion layer. (b) Stable contact between the Au electrode layer and the PA-PdNWs was formed. The structures shown in these images are the case of Cu thickness = 80 nm, Pd thickness = 70 nm, and Au thickness = 300 nm.

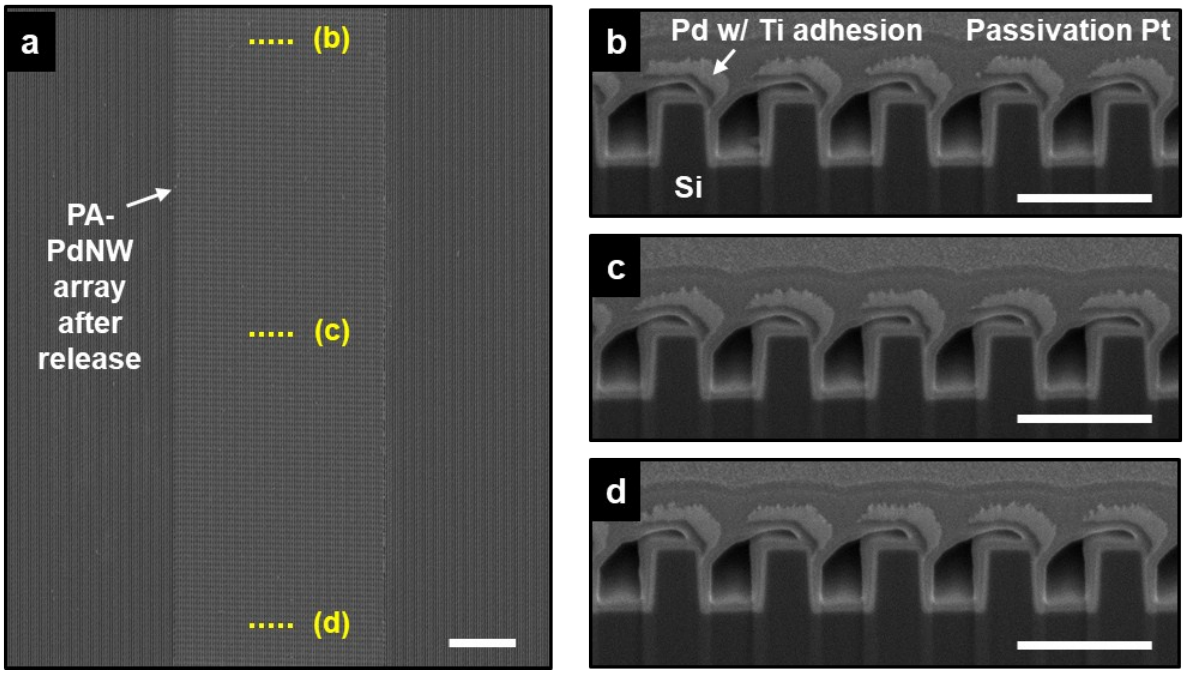

Figure S3. SEM images of the PA-PdNW array with Pd thickness of 70 nm after Cu sacrificial layer etching (a) A top view (Scale bar = 10 µm) of PA-PdNW array without Au electrodes. (b-d) Cross-sectional views of the uniformly suspended PA-PdNW after Cu sacrificial layer removal captured along 100 µm distance (Scale bars = 500 nm).

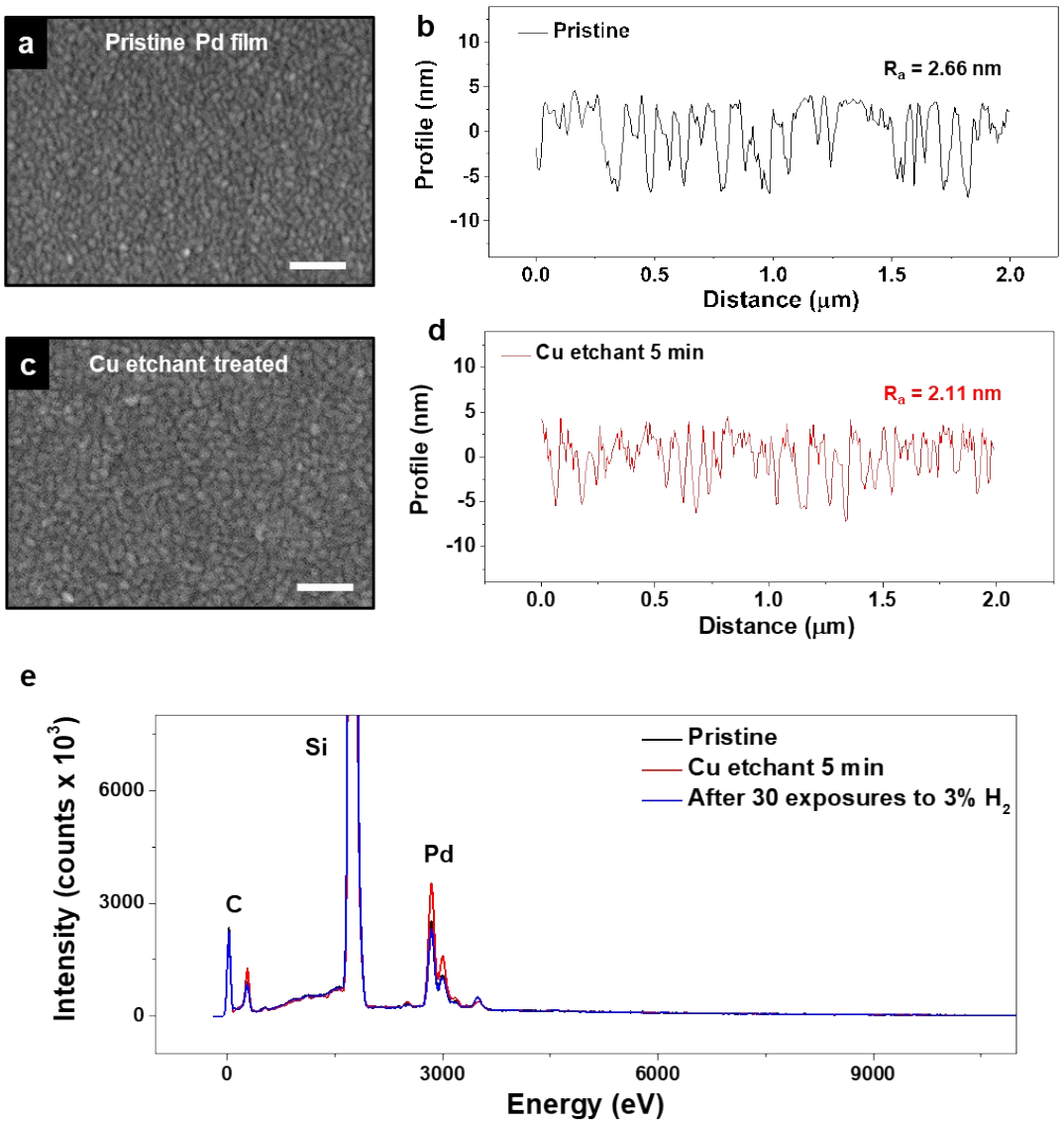

Figure S4. SEM images and surface profiles measured by atomic force microscopy (AFM) of (a-b) a pristine Pd film (Scale bars = 100 nm) and (c-d) a Pd film after 5 min Cu etchant. No morphological change was found during the Cu removal. (e) Atomic composition of a Pd film at its pristine state, after 5 min Cu etchant treatment, and after 30 exposures to 3% H_2 measured by energy dispersive spectroscopy (EDS). No meaningful change in atomic composition was found. It could be inferred that chemical composition of PA-PdNWs remained unchanged during the fabrication and sensor measurements.

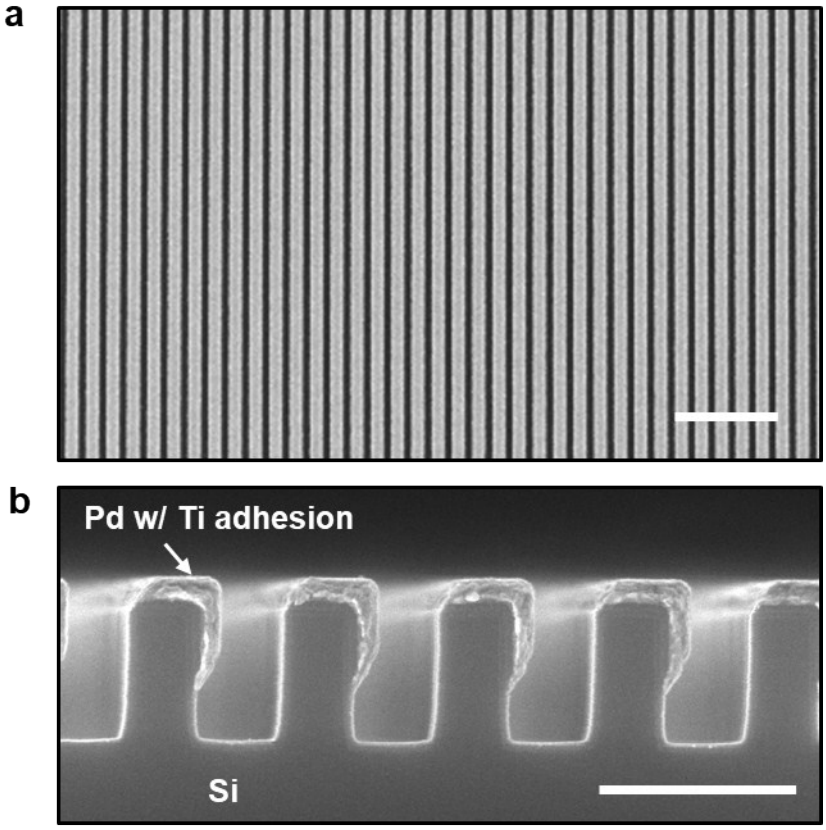

Figure S5. SEM images of the fabricated FA-PdNW array with Pd thickness of 70 nm. (a) A top view (Scale bar = 2 μm) and (b) a cross-section view (Scale bar = 500 nm) of the fabricated FA-PdNW array.

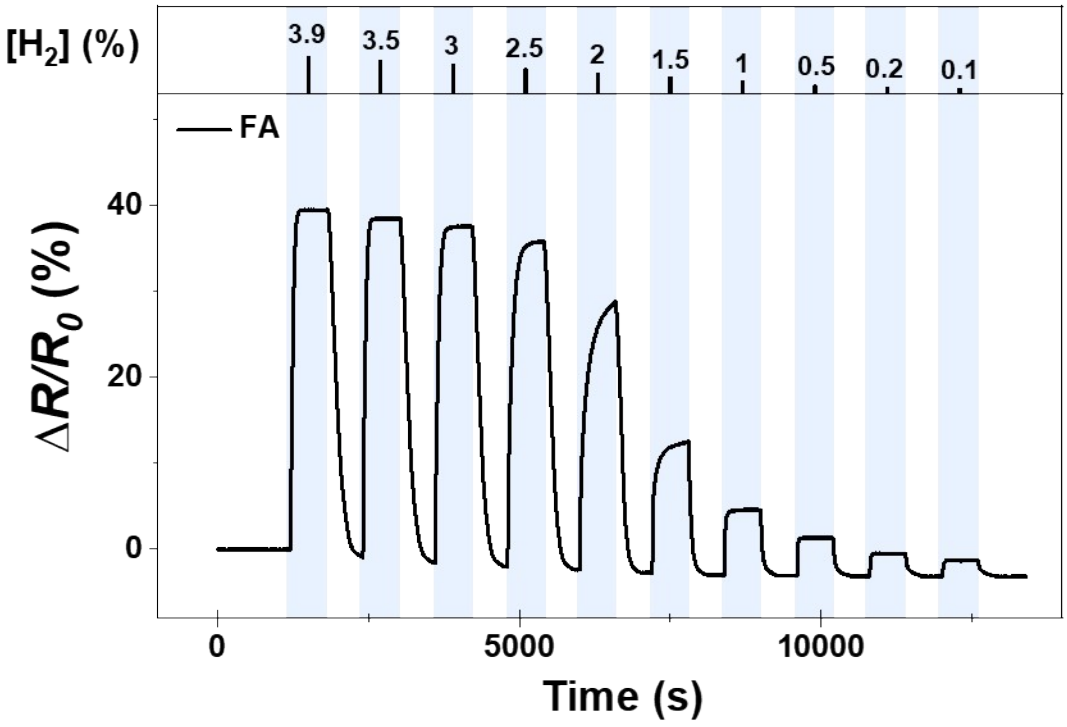

Figure S6. A representative response curve of FA-PdNW sensors according to various H_2 concentrations. Pd thickness = 70 nm, wire length = 20 μm, width of nanowire array = 30 μm.

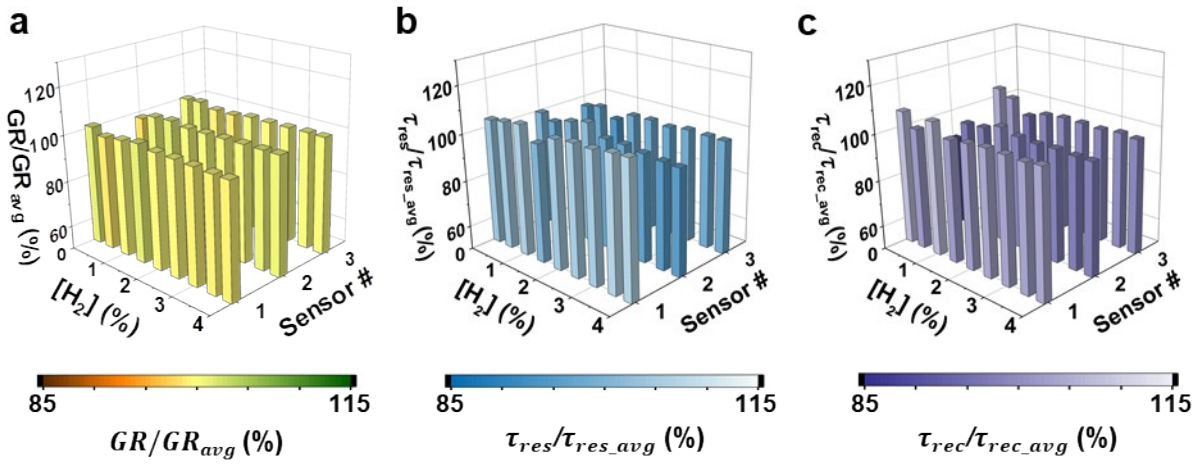

Figure S7. Performance variation between different sensors with the same geometrical specifications of the PA-PdNW array sensing part (Pd thickness ~70 nm, Cu sacrificial thickness ~110 nm). All performance indexes resides within 15% deviation from the average for all measured concentration range (0.1 – 3.9% H_2) (a) Gas response ($GR=\Delta R/R_{air}$), (b) response time, and (c) recovery time, respectively.

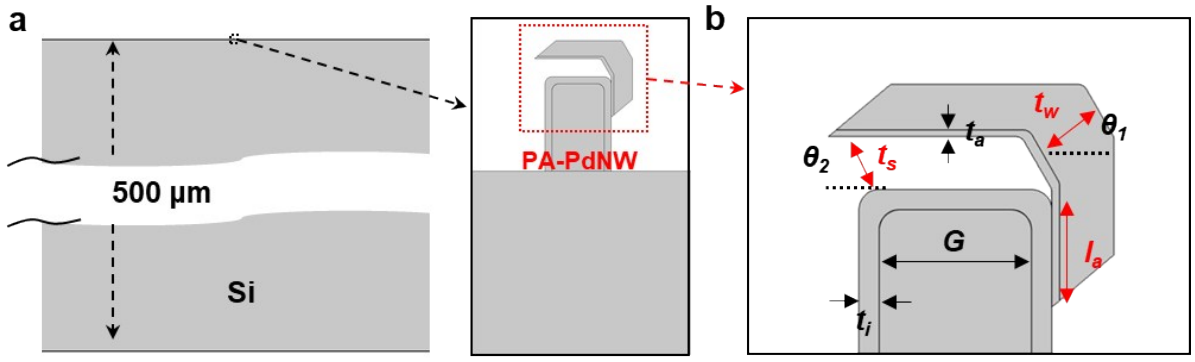

Figure S8. Cross-sectional geometrical model used in FEM calculation of von Mises stress of a PA-PdNW. The simulation thickness (depth = wire length direction) had no influence on calculated stress values and was set to be 1 m. (a) A real-scale simulation model of a PA-PdNW (red-dotted box). The bottom of Si substrate was set as a fixed constraint. (b) Geometrical parameters related to the shape of a PA-PdNW where t_w: Pd thickness, t_a: adhesion Ti thickness (10 nm), t_s: Cu sacrificial layer thickness, t_i: Al_2O_3 insulating layer thickness (20 nm), G: Grating width (150 nm), P: Grating pitch (400 nm) θ_1: Pd deposition angle (30°), θ_2: Cu deposition angle (60°), l_a: anchored length. Black-colored parameters are fixed, and red-colored parameters are the variables closely related to the decision of von-Mises stress. The model was figured based on the directional flux properties of the oblique angle deposition process using trigonometrical relations. l_a can be expressed as a function of t_s with the following relationship, $l_a = (P - G - t_i - t_s\cos\theta_2)\tan\theta_1 - t_s\sin\theta_2 = f(t_s)$, and t_w is independent from the others. Thus, the maximum stress calculations depicted in Figure 3b were conducted with varying t_w and l_a.

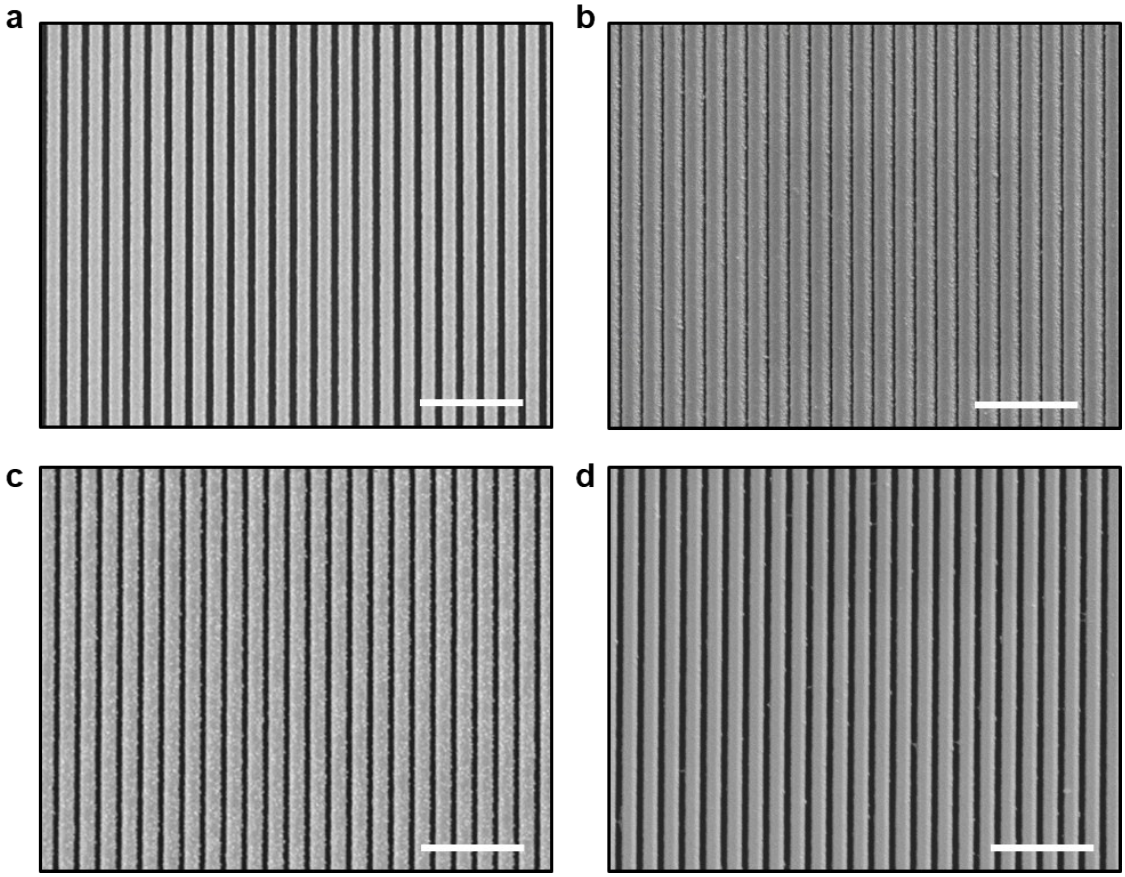

Figure S9. SEM images viewed from the top (Scale bars = 2 μm) of the fabricated various Pd nanowires with different wire thickness (t_w) and anchored length (l_a) of which reliability were compared in Figure 3. (a) FA-PdNW of $t_w \sim 70\ nm$, (b) PA-PdNW of $t_w \sim 140\ nm$ and $l_a \sim 90\ nm$, (c) PA-PdNW of $t_w \sim 70\ nm$ and $l_a \sim 90\ nm$, (d) PA-PdNW of $t_w \sim 20\ nm$ and $l_a \sim 50\ nm$.

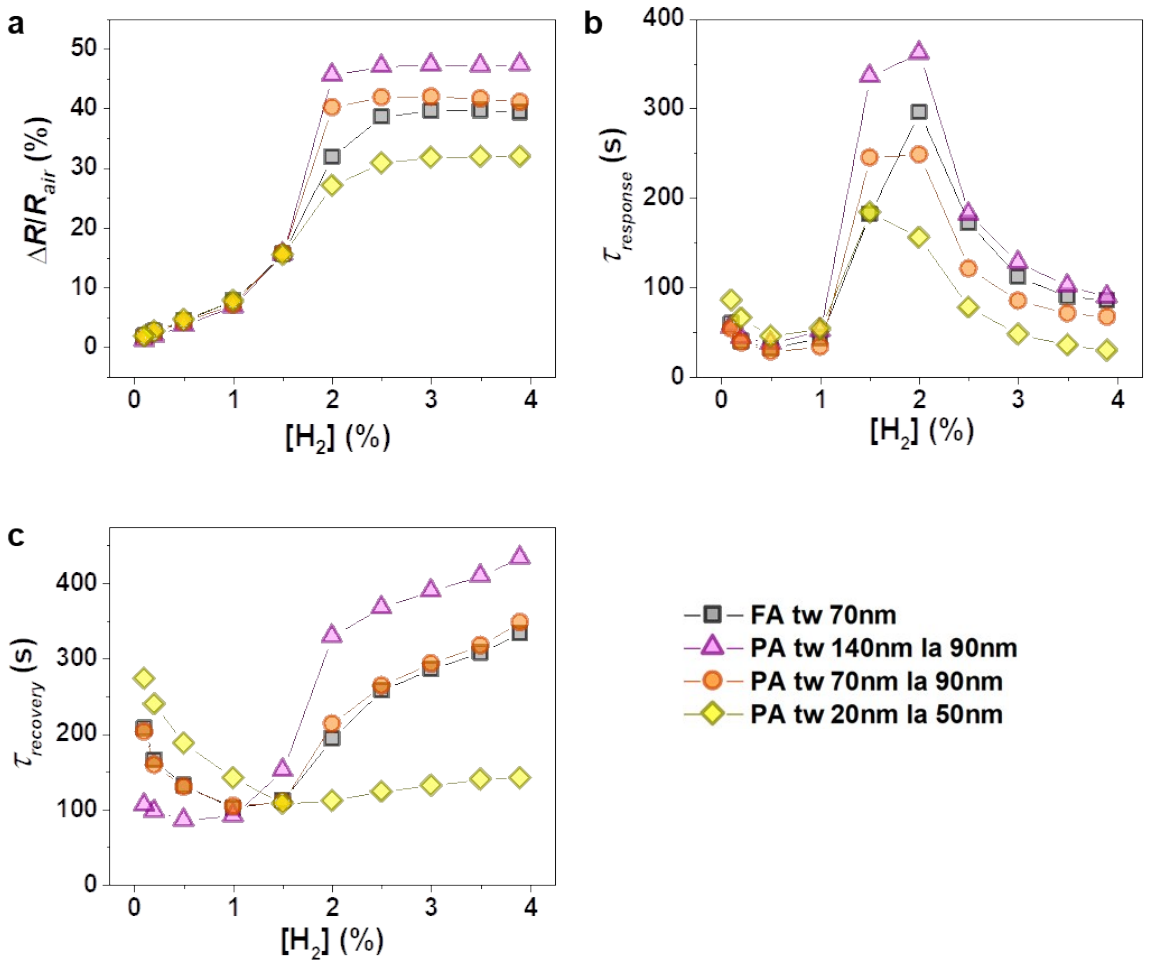

Figure S10. Sensing performance of the fabricated Pd nanowires with different wire thickness (t_w) and anchored length (l_a) of which reliability were compared in Figure 3. (a) Gas response, (b) response time, (c) recovery time, respectively. As the wire thickness gets thinner, the sensitivities and the response times tended to decrease due to the nanowire size effect.[S1]

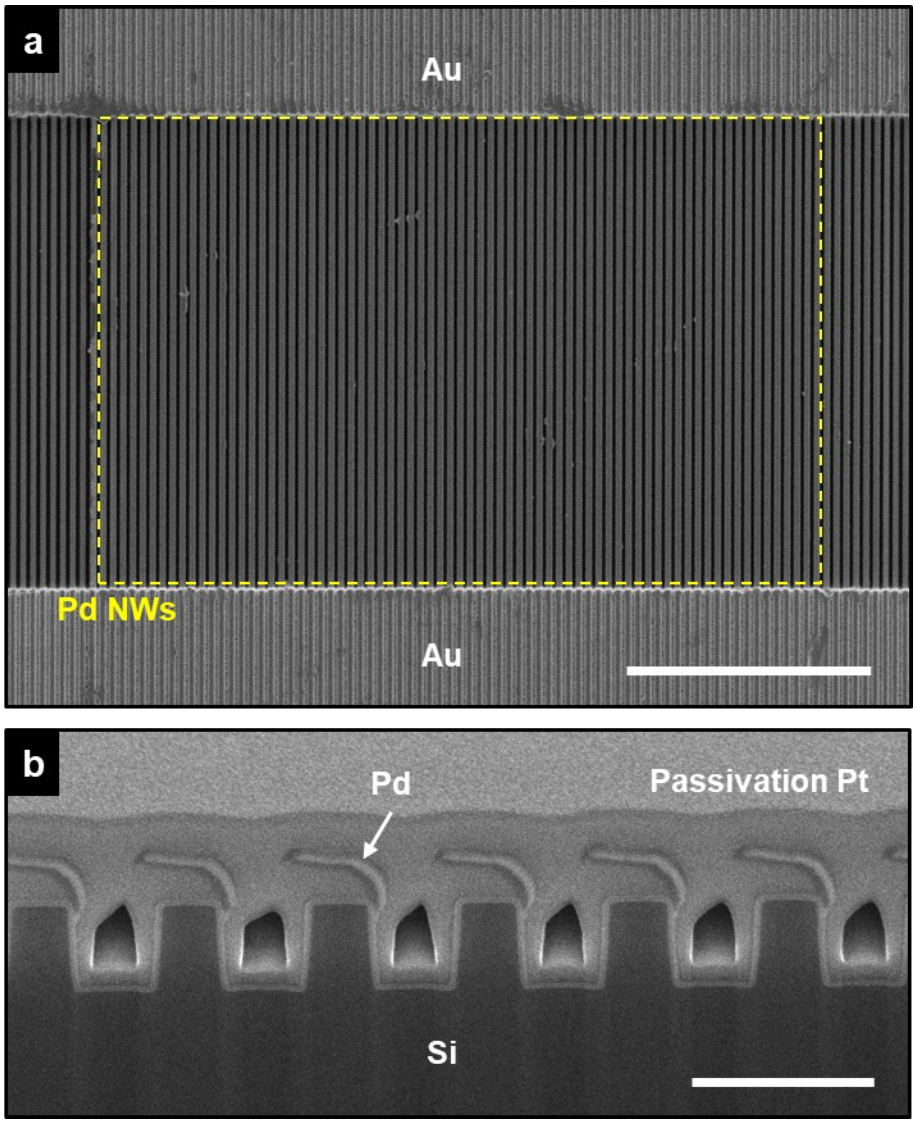

Figure S11. (a) A top-viewed (Scale bar = 10 μm) and (b) a cross-sectional (Scale bar = 500 nm) SEM image of PA-PdNW array (t_w~20 nm, l_a~50 nm) after 300 times of β-phase transitions. No severe structural destructions were observed (only manufacturing defects such as particles and roughened lift-off edge were found), and air-suspended and partially anchored characteristics of the Pd wires were stably preserved.

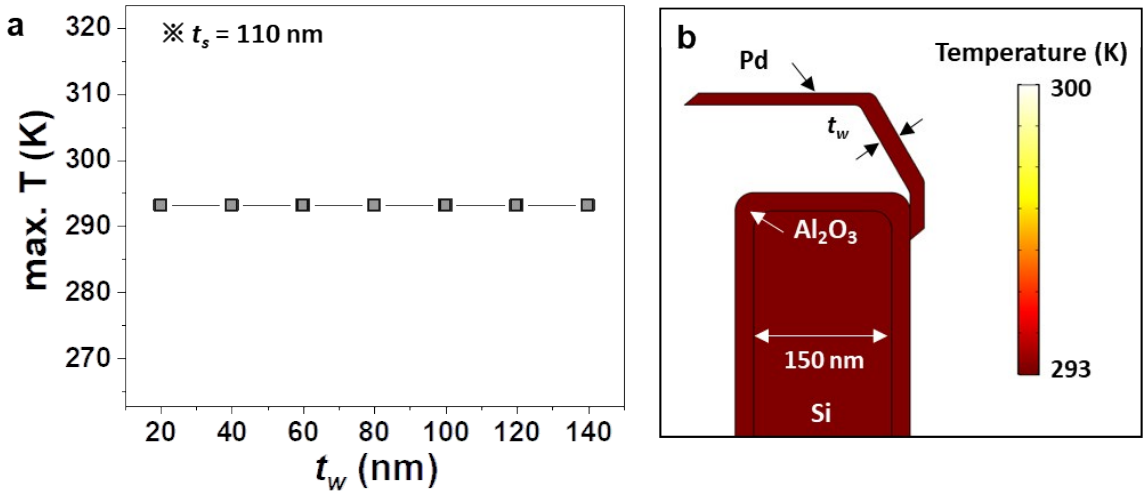

Figure S12. Identification of Joule-heating effect by FEM simulation. Only results of t_s = 110 nm cases were shown which have the shortest anchored region and thus have the narrowest heat sink path. Current density flowing through a Pd nanowire was set as the following equation. $J = I_{bias}/t_w \times w_{wire} \times n_{wire}$, I_{bias} = 1mA, w_{wire} = 150 nm, n_{wire} = 75. Simulated results of (a) the maximum temperature according to varying t_w and (b) the cross-sectional temperature distribution of the case of t_w = 20 nm corresponding to the highest current density. There was no temperature rise.

Sensing element	Dimensions (nm)	T (K)	$\Delta R/R_{air}$ (%) @ $[H_2] \approx 4\%$	$\Delta R/R_{air}$ (%) @ $[H_2] \approx 0.1\%$	τ_{resp}/τ_{rec} (s) @ $[H_2] \approx 4\%$	τ_{resp}/τ_{rec} (s) @ $[H_2] \approx 0.1\%$
This work, PA-PdNW	t_w = 140	RT	47.4	1.14	90 / 434	56 / 106
	t_w = 70	RT	41.1	1.86	67.3 / 349	54 / 203
	t_w = 20	RT	32	1.85	30 / 142	86 / 274
	t_w = 20 (@ 85% RH)	RT	31.7	2.14	146 / 326	194 / 100
This work, FA-PdNW	t_w = 70	RT	39.4	1.91	86 / 334	60 / 208
Pd nanowire[S2]	33 (h) x 47 (w)	RT	15	2	30 / 100	40 / 300
Pd nanowire[S3]	27 (h) x 75 (w)	RT	10.8	1.8	40 / 180	90 / 550
Pd nanowire[S3]	27 (h) x 75 (w)	428	0.75	0.06	2 / 6	7 / 15
Pd nanonetwork[S4]	D = 17	RT	11	1.9	20 / NR	120 / NR
Pt coated (θ_{Pt}=1 ML) Pd nanowire[S5]	40 (h) x 100 (w)	RT	11.5	-	35 / 50	250 / 15

Table S1. H_2 sensing characteristics of Pd nanowire based gas sensors.

References for supplementary information

S1 K. J. Jeon, J. M. Lee, E. Lee and W. Lee, *Nanotechnology*, 2009, **20**, 135502.

S2 F. Yang, D. K. Taggart and R. M. Penner, *Nano Lett.*, 2009, **9**, 2177–2182.

S3 F. Yang, D. K. Taggart and R. M. Penner, *Small*, 2010, **6**, 1422–1429.

S4 X. Q. Zeng, M. L. Latimer, Z. L. Xiao, S. Panuganti, U. Welp, W. K. Kwok and T. Xu, *Nano Lett.*, 2011, **11**, 262–268.

S5 X. Li, Y. Liu, J. C. Hemminger and R. M. Penner, *ACS Nano*, 2015, **9**, 3215–3225.